Int. J. Solids Structures, 1974, *Vol.* 10, pp. 503–517. Pergamon Press. Printed in Gt. Britain.

STRESS DISTRIBUTION IN A LAP JOINT UNDER TENSION-SHEAR

DICK J. CHANG† and R. MUKI

Mechanics and Structures Department, School of Engineering and Applied Science, University of California, Los Angeles, CA 90024, U.S.A.

(*Received* 27 *June* 1973; *revised* 21 *September* 1973)

Abstract—This paper deals with the elastostatic load transfer of a tensile load in a model of an adhesive lap joint (tension-shear problem). The adhesive layer is regarded as infinitesimally thin and the displacement and traction vectors in the adherends are assumed to be continuous across the bond. The problem is reduced to a pair of Fredholm integral equations of the second kind which involve the mean angle between the deformed bond line and the tensile load. This angle, in turn, is determined by means of a scheme due to Goland and Reissner. Numerical results for the bond line stresses and the stress intensity factors at the ends of the bonded region are presented.

INTRODUCTION

In this paper the adherends are modeled by two parallel, infinite strips of equal constant thickness, bonded along a common finite line. The bond is assumed to be infinitesimally thin and the bond-line tractions and displacements are taken to be continuous from one adherend to the other. The two-dimensional stress and displacement fields are determined within the scope of the linear elasticity theory of plane strain in this model of an adhesive lap joint, which is subjected to tension-shear type loading.

Section 1 contains auxiliary solutions for a slab under a concentrated normal and tangential edge load, respectively. Section 2 is devoted to the formulation of the "inner problem". By "inner problem", we mean the determination of stresses in the lap joint when the magnitude and direction of the force transmitted through the bond is given. With the aid of the two auxiliary solutions in Section 1, the problem is reduced to a coupled pair of Cauchy-type singular integral equations subject to two normalizing conditions. Fortunately, this pair of singular integral equations may be uncoupled by means of the normalizing conditions and the symmetry properties of the bond stresses. Section 4 is concerned with the determination of the angle of rotation of the bond line relative to the applied load. The analysis is based on a paper by Goland and Reissner[1]. Finally, illustrative numerical results are presented in Section 5. In particular the dependence of the stress intensity factors upon the loading parameter and joint geometry is shown.

1. *Auxiliary results*

As a prerequisite for the formulation, we record here certain results for an elastic slab in a state of plane strain. Consider an elastic slab of Young's modulus E, and Poisson's ratio ν, the median section of which occupies the region

$$D = \{(x_1, x_2) \mid -\infty < x_1 < \infty, \qquad -b \leq x_2 \leq b\}. \tag{1}$$

† Present address: The Aerospace Corporation, El Segundo, CA 90245, U.S.A.

Now suppose that the slab is subjected to a normal (tangential) edge load of unit magnitude per unit length in x_3-direction situated at $(0, -b)$ and applied in the positive x_2-direction (in the positive x_1-direction). Further, denote by $\overset{(\gamma)}{u_\alpha}$, $\overset{(\gamma)}{\varepsilon_{\alpha\beta}}$ and $\overset{(\gamma)}{\tau_{\alpha\beta}}$ $(\alpha, \beta, \gamma = 1, 2)$ the cartesian components of displacement, strain and stress in the slab under such a loading (superscript (1) for normal, and superscript (2) for tangential loading) subject to the regularity requirements

$$\left.\begin{aligned} &\overset{(\gamma)}{\tau_{\alpha\beta}}(x_1, x_2) = o(|x_1|^{\lambda}) \quad \text{as} \quad x_1 \to -\infty, \\ &\overset{(\gamma)}{\tau_{\alpha\beta}}(x_1, x_2) = o(e^{-\varepsilon x_1}) \quad \text{as} \quad x_1 \to \infty, \end{aligned}\right\} \tag{2}$$

for some positive λ and ε.

Then, after routine manipulation based on Airy's stress function and the exponential Fourier transform, one arrives at

$$\begin{aligned}
\overset{(1)}{\tau_{11}}(x_1, x_2) &= \frac{3x_1x_2}{4b^3} + \frac{1}{\pi}\int_0^\infty \Big\{\big[(-bsS_-(bs) + C_-(bs) - x_2 sS_+(bs))\sinh(x_2 s) \\
&\quad + (bsC_+(bs) - S_+(bs) + x_2 sC_-(bs))\cosh(x_2 s)\big]\cos(x_1 s) - \frac{3x_2}{2b^3 s^2}\Big\}\,ds, \\
\overset{(1)}{\tau_{22}}(x_1, x_2) &= \frac{1}{\pi}\int_0^\infty \big[(bsS_-(bs) + C_-(bs) + x_2 sS_+(bs))\sinh(x_2 s) \\
&\quad - (bsC_+(bs) + S_+(bs) + x_2 sS_-(bs))\cosh(x_2 s)\big]\cos(x_1 s)\,ds, \\
\overset{(1)}{\tau_{12}}(x_1, x_2) &= \frac{3}{8b}\left(1 - \frac{x_2^2}{b^2}\right) + \frac{1}{\pi}\int_0^\infty \big[(bsC_-(bs) + x_2 sC_+(bs))\sinh(x_2 s) \\
&\quad - (bsS_+(bs) + x_2 sS_-(bs))\cosh(x_2 s)\big]\sin(x_1 s)\,ds, \qquad (3) \\
\overset{(2)}{\tau_{11}}(x_1, x_2) &= \frac{1}{4b}\left(1 - \frac{3x_2}{b}\right) + \frac{1}{\pi}\int_0^\infty \big[(x_2 sS_-(bs) - 2C_+(bs) + bsS_+(bs))\cosh(x_2 s) \\
&\quad + (-x_2 sC_+(bs) + 2S_-(bs) - bsC_-(bs))\sinh(x_2 s)\big]\sin(x_1 s)\,ds, \\
\overset{(2)}{\tau_{22}}(x_1, x_2) &= \frac{1}{\pi}\int_0^\infty \big[(bsC_-(bs) + x_2 sC_+(bs))\sinh(x_2 s) \\
&\quad - (bsS_+(bs) + x_2 sS_-(bs))\cosh(x_2 s)\big]\sin(x_1 s)\,ds, \\
\overset{(2)}{\tau_{12}}(x_1, x_2) &= \frac{1}{\pi}\int_0^\infty \big[(C_+(bs) - bsS_+(bs) - x_2 sS_-(bs))\sinh(x_2 s) \\
&\quad - (S_-(bs) - bsS_-(bs) - x_2 sC_+(bs))\cosh(x_2 s)\big]\cos(x_1 s)\,ds,
\end{aligned}$$

where

$$\begin{aligned}
C_+(s) &= \frac{\cosh s}{\sinh(2s) + 2s}, \quad S_+(s) = \frac{\sinh s}{\sinh(2s) + 2s}, \\
C_-(s) &= \frac{\cosh s}{\sinh(2s) - 2s}, \quad S_-(S) = \frac{\sinh s}{\sinh(2s) - 2s}.
\end{aligned} \tag{4}$$

Further, we present here the displacements along the lower edge, needed later, which were obtained from (3) and the stress–displacement relations.

$$\frac{\partial u_1^{(1)}}{\partial x_1}(x_1, -b) = -\frac{(1+\nu)(1-2\nu)}{\pi E}\delta(x_1) + \frac{1-\nu^2}{\pi E}\left\{-\frac{3\pi x_1}{4b^2} + 2\int_0^\infty \left[f_1(bs)\cos(x_1 s) + \frac{3}{4b^2 s^2}\right] ds\right\},$$

$$\frac{\partial u_2^{(1)}}{\partial x_1}(x_1, -b) = \frac{2(1-\nu^2)}{\pi E}\left\{-\frac{1}{x_1} - \frac{3\pi x_1^2}{16b^3} + \frac{3\pi}{10b} - \int_0^\infty \left[f_2(bs)\sin(x_1 s) - \frac{3x_1}{4b^3 s^2}\right] ds\right\}, \tag{5}$$

$$\frac{\partial u_1^{(2)}}{\partial x_1}(x_1, -b) = \frac{1-\nu^2}{\pi E}\left\{\frac{\pi}{b} - \frac{2}{x_1} + 2\int_0^\infty f_3(bs)\sin(x_1 s)\, ds\right\},$$

$$\frac{\partial u_2^{(2)}}{\partial x_1}(x_1, -b) = \frac{(1+\nu)(1-2\nu)}{\pi E}\delta(x_1) + \frac{1-\nu^2}{\pi E}\left\{\frac{3\pi x_1}{4b^2} - 2\int_0^\infty \left[f_1(bs)\cos(x_1 s) + \frac{3}{4b^2 s^2}\right] ds\right\}.$$

where $\delta(x)$ stands for the delta function and

$$f_1(s) = s\left[\frac{1}{\sinh(2s) + 2s} - \frac{1}{\sinh(2s) - 2s}\right],$$

$$f_2(s) = -\frac{2s + 1 - e^{-2s}}{2[\sinh(2s) + 2s]} + \frac{2s + 1 + e^{-2s}}{2[\sinh(2s) - 2s]}, \tag{6}$$

$$f_3(s) = \frac{2s - 1 - e^{-2s}}{2[\sinh(2s) + 2s]} - \frac{2s - 1 + e^{-2s}}{2[\sinh(2s) - 2s]}.$$

The above expressions (5) were obtained, as in [2], by decomposing each integral representation into a part uniformly convergent in D and one which is analytically integrable, and then taking the limit as x_2 tends to $-b$.

2. *Formulation of the problem*

We turn now to the formulation of the tension-shear problem. The configuration of the joint before the application of the load is shown in Fig. 1. Note that a new rectangular cartesian coodinate system $\bar{X}_i$ has been introduced with the origin at the center of the bond line.

Assume now that a uniform tensile stress $\sigma_{11} = P/2b$ is applied to the upper and lower plate at $\bar{X}_1 = -\infty$ and $\bar{X}_1 = +\infty$. Under this loading the joint deforms as shown in Fig. 2 and the plane tangent to the bond plane at the origin rotates about the $\bar{X}_3$ axis. This angle of rotation will be determined in the next section by use of the Goland–Reissner analysis. In the remainder of this section, we assume that the angle of rotation is known and designate it by $\hat{\theta}$.

Our next task is to reduce the problem to a pair of integral equations. Referring to the coordinate system in Fig. 1, we denote the displacements and stresses in the plate by u_α^+, u_α^- and $\tau_{\alpha\beta}^+$, $\tau_{\alpha\beta}^-$ where $+$ $(-)$ denotes the upper (lower) plate.

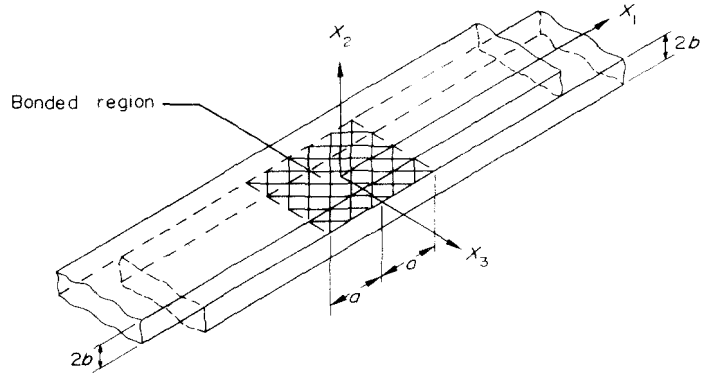

Fig. 1. Geometry of adhesive joint.

Then, the boundary conditions and the bond conditions become

$$\begin{aligned}
&\tau^{+}_{2\alpha}(\bar{X}_1, 2b) = 0, \quad \tau^{-}_{2\alpha}(\bar{X}_1, -2b) = 0 \qquad \bar{X}_1 \in (-\infty, \infty),\\
&\tau^{+}_{2\alpha}(\bar{X}_1, 0) = 0, \quad \tau^{-}_{2\alpha}(\bar{X}_1, 0) = 0 \qquad |\bar{X}_1| \in (a, \infty),\\
&u^{+}_{\alpha}(\bar{X}_1, 0) = u^{-}_{\alpha}(\bar{X}_1, 0), \quad \tau^{+}_{2\alpha}(\bar{X}_1, 0) = \tau^{-}_{2\alpha}(\bar{X}_1, 0) \qquad \bar{X}_1 \in (-a, a),
\end{aligned} \tag{7}$$

while the regularity requirements are

$$\begin{aligned}
&\tau^{+}_{\alpha\beta}(\bar{X}_1, \bar{X}_2) = o(1) \quad \text{as} \quad \bar{X}_1 \to \infty,\\
&\tau^{-}_{\alpha\beta}(\bar{X}_1, \bar{X}_2) = o(1) \quad \text{as} \quad \bar{X}_1 \to -\infty.
\end{aligned} \tag{8}$$

In addition the normalization condition can be stated as

$$\begin{aligned}
&\int_{-a}^{a} \tau^{+}_{22}(\bar{X}_1, 0)\, \mathrm{d}\bar{X}_1 = \int_{-a}^{a} \tau^{-}_{22}(\bar{X}_1, 0)\, \mathrm{d}\bar{X}_1 = P \sin\hat{\theta},\\
&\int_{-a}^{a} \tau^{+}_{12}(\bar{X}_1, 0)\, \mathrm{d}\bar{X}_1 = \int_{-a}^{a} \tau^{-}_{12}(\bar{X}_1, 0)\, \mathrm{d}\bar{X}_1 = -P \cos\hat{\theta}.
\end{aligned} \tag{9}$$

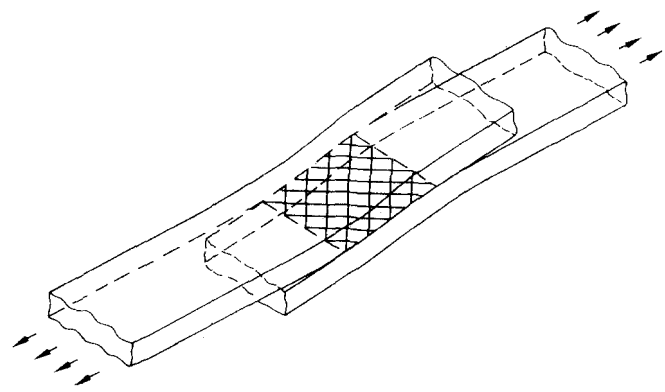

Fig. 2. Deformed configuration of the joint.

Since the upper and lower plates have the same geometry and elastic properties, the tension shear loading will produce (See Figs. 1 and 2) a displacement field such that

$$u_\alpha^+(\bar{X}_1, \bar{X}_2) = -u_\alpha^-(-\bar{X}_1, -\bar{X}_2) \qquad \bar{X}_1 \in (-\infty, \infty), \qquad \bar{X}_2 \in (0, 2b). \tag{10}$$

In particular, (10) together with the fifth of (7) gives

$$u_\alpha^+(\bar{X}_1, 0) = -u_\alpha^+(-\bar{X}_1, 0) \qquad \bar{X}_1 \in (-a, a). \tag{11}$$

Now consider an elastic field in the upper plate, say $\tilde{u}_\alpha^+$, $\tilde{\tau}_{\alpha\beta}^+$, which satisfies all the boundary, regularity and normalization conditions: the first four of (7), (8) and (9). Further, assume $\tilde{u}_\alpha^+$, $\tilde{\tau}_{\alpha\beta}^+$ satisfy the condition (11) instead of the last two of (7). Now extend the elastic field in the upper plate into the lower plate as follows:

$$\begin{aligned} &\tilde{u}_\alpha^-(\bar{X}_1, \bar{X}_2) = -\tilde{u}_\alpha^+(-\bar{X}_1, -\bar{X}_2), \\ &\tilde{\tau}_{\alpha\beta}^-(\bar{X}_1, \bar{X}_2) = \tilde{\tau}_{\alpha\beta}^+(-\bar{X}_1, -\bar{X}_2) \qquad \bar{X}_1 \in (-\infty, \infty), \bar{X}_2 \in (-2b, 0). \end{aligned} \tag{12}$$

It can be verified that the fields $\tilde{u}_\alpha$, $\tilde{\tau}_{\alpha\beta}$ satisfy all the required conditions. Accordingly in the following it is only necessary to deal with the upper plate.

We therefore restrict our discussion to the upper plate and remove the superscript " + ". On the basis of the preceding argument u_α and $\tau_{\alpha\beta}$, referring to the coordinate system in Fig. 3, must meet the conditions:

$$\begin{aligned} &\tau_{2\alpha}(x_1, b) = 0 \qquad x_1 \in (-\infty, \infty), \\ &\tau_{2\alpha}(x_1, -b) = 0 \qquad |x_1| \in (a, \infty), \\ &u_\alpha(x_1, -b) = -u_\alpha(-x_1, -b) \qquad x_1 \in (-a, a). \end{aligned} \tag{13}$$

$$\begin{aligned} &\tau_{\alpha\beta}(x_1, x_2) \overset{(2)}{=} O(1) \quad \text{as} \quad x_1 \to -\infty, \\ &\tau_{\alpha\beta}(x_1, x_2) = o(1) \quad \text{as} \quad x_1 \to \infty, \end{aligned} \tag{14}$$

$$\begin{aligned} &\int_{-a}^{a} \tau_{22}(x_1, \overset{(2)}{=} b)\, \mathrm{d}x_1 = P \sin \hat{\theta}, \\ &\int_{-a}^{a} \tau_{12}(x_1, -b)\, \mathrm{d}x_1 = -P \cos \hat{\theta}. \end{aligned} \tag{15}$$

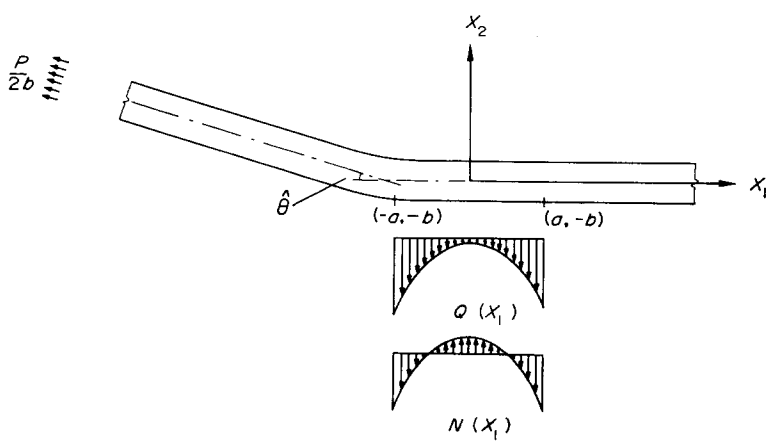

Fig. 3. Upper plate–loading and coordinate system.

At this point we introduce new symbols N and Q through

$$\begin{aligned} N(x_1) &= \tau_{22}(x_1, -b), \\ Q(x_1) &= -\tau_{12}(x_1, -b) \qquad x_1 \in (-a, a). \end{aligned} \tag{16}$$

Then, by means of integral superposition, the stresses $\tau_{\alpha\beta}$ in the upper plate can be expressed in terms of the auxiliary stress fields $\overset{(1)}{\tau}_{\alpha\beta}$ and $\overset{(2)}{\tau}_{\alpha\beta}$ established in Section 1 as follows:

$$\tau_{\alpha\beta}(x_1, x_2) = -\int_{-a}^{a} \overset{(1)}{\tau}_{\alpha\beta}(x_1 - t, x_2)N(t)\,dt + \int_{-a}^{a} \overset{(2)}{\tau}_{\alpha\beta}(x_1 - t, x_2)Q(t)\,dt \qquad (x_1, x_2) \in D. \tag{17}$$

Use of integral superposition as in (17), and differentiation of the third equation in (13) with respect to x_1, gives

$$\begin{aligned} &-\int_{-a}^{a} \frac{\partial \overset{(1)}{u}_1}{\partial x_1}(x_1 - t, -b)N(t)\,dt + \int_{-a}^{a} \frac{\partial \overset{(2)}{u}_1}{\partial x_1}(x_1 - t, -b)Q(t)\,dt \\ &= -\int_{-a}^{a} \frac{\partial \overset{(1)}{u}_1}{\partial x_1}(-x_1 - t, -b)N(t)\,dt + \int_{-a}^{a} \frac{\partial \overset{(2)}{u}_1}{\partial x_1}(-x_1 - t, -b)Q(t)\,dt, \\ &-\int_{-a}^{a} \frac{\partial \overset{(1)}{u}_2}{\partial x_1}(x_1 - t, -b)N(t)\,dt + \int_{-a}^{a} \frac{\partial \overset{(2)}{u}_2}{\partial x_1}(x_1 - t, -b)Q(t)\,dt \\ &= -\int_{-a}^{a} \frac{\partial \overset{(1)}{u}_2}{\partial x_1}(-x_1 - t, -b)N(t)\,dt + \int_{-a}^{a} \frac{\partial \overset{(2)}{u}_2}{\partial x_1}(-x_1 - t, -b)Q(t)\,dt \qquad x_1 \in (-a, a). \end{aligned} \tag{18}$$

By use of (5), (15), (16) and in view of the fact that N and Q are symmetric (even) with respect to the origin, equations (18) may be reduced to

$$\begin{aligned} \int_{-a}^{a} \frac{Q(t)}{t - x_1}\,dt &= \psi_1(x_1), \\ \int_{-a}^{a} \frac{N(t)}{t - x_1}\,dt &= \psi_2(x_1) \qquad x_1 \in (-a, a), \end{aligned} \tag{19}$$

where

$$\begin{aligned} \psi_1(x_1) &= \int_{-a}^{a} \left\{ \int_0^{\infty} f_3(bs)\sin[(x_1 - t)s]\,ds \right\} Q(t)\,dt - \frac{3\pi}{8b^2}\,x_1 P \sin\hat{\theta}, \\ \psi_2(x_1) &= \int_{-a}^{a} \left\{ \int_0^{\infty} \left[f_2(bs)\sin[(x_1 - t)s] - \frac{3(x_1 - t)}{4b^3 s^2} \right] ds \right\} N(t)\,dt + \frac{3\pi}{8b^2}\,x_1 P \cos\hat{\theta}, \end{aligned} \tag{20}$$

in which f_2, f_3 are defined by (6). Observe that the integral equations (19) are not coupled, in contrast to (18).

3. *Reduction of the problem to a pair of Fredholm integral equations*

Our next objective is to reduce each of the singular integral equations (19) to a standard Fredholm integral equation by means of Muskhelishvili's method ([3], p.235). In this manner one finds from (19) that

$$Q(t_0) = -\frac{1}{\pi^2\sqrt{a^2-t_0^2}}\left[\int_{-a}^{a}\frac{\sqrt{a^2-t^2}}{t-t_0}\cdot\psi_1(t)\,dt + A_1\right],$$
$$N(t_0) = -\frac{1}{\pi^2\sqrt{a^2-t_0^2}}\left[\int_{-a}^{a}\frac{\sqrt{a^2-t^2}}{t-t_0}\cdot\psi_2(t)\,dt + A_2\right] \qquad t_0\in(-a,a), \tag{21}$$

where A_1 and A_2 are undetermined constants.

To determine the constants A_1 and A_2, substitute from (16) into (15) and then for Q and N from (21) into the resulting integral relations. After carrying out the integrations involved, one has

$$A_1 = -\pi P\cos\hat{\theta},$$
$$A_2 = -\pi P\sin\hat{\theta}. \tag{22}$$

An inspection of the integral equations (21) suggests the introduction of new dimensionless variables through

$$\xi = t_0/b,$$
$$\hat{Q}(\xi) = b\sqrt{\alpha^2-\xi^2}\cdot Q(b\xi)/P, \tag{23}$$
$$\hat{N}(\xi) = b\sqrt{\alpha^2-\xi^2}\cdot N(b\xi)/P.$$

where

$$\alpha = a/b. \tag{24}$$

Then, after a permissible interchange of the order of integration and in view of (22), we arrive at the integral equations for $\hat{Q}$ and $\hat{N}$:

$$\hat{Q}(\xi) + \int_{-\alpha}^{\alpha} K_1(\xi,\eta)\hat{Q}(\eta)\,d\eta = P_1(\xi),$$
$$\hat{N}(\xi) + \int_{-\alpha}^{\alpha} K_2(\xi,\eta)\hat{N}(\eta)\,d\eta = P_2(\xi) \qquad \xi\in[-\alpha,\alpha]. \tag{25}$$

where

$$K_1(\xi,\eta) = \frac{1}{\pi^2\sqrt{\alpha^2-\eta^2}}\int_{-\alpha}^{\alpha}\frac{\sqrt{\alpha^2-\zeta^2}}{\zeta-\xi}\cdot G_1(\zeta-\eta)\,d\zeta,$$
$$K_2(\xi,\eta) = \frac{1}{\pi^2\sqrt{\alpha^2-\eta^2}}\int_{-\alpha}^{\alpha}\frac{\sqrt{\alpha^2-\zeta^2}}{\zeta-\xi}\cdot G_2(\zeta-\eta)\,d\zeta,$$
$$P_1(\xi) = \frac{\cos\hat{\theta}}{\pi} + \frac{3}{16}(\alpha^2-2\xi^2)\sin\hat{\theta}, \tag{26}$$
$$P_2(\xi) = \frac{\sin\hat{\theta}}{\pi} - \frac{3}{16}(\alpha^2-2\xi^2)\cos\hat{\theta}.$$

The functions G_1 and G_2 are defined by

$$G_1(\xi) = \int_0^{\infty} f_3(s)\sin(\xi s)\,ds,$$
$$G_2(\xi) = \int_0^{\infty}\left[f_2(s)\sin(\xi s) + \frac{3\xi}{4s^2}\right]ds \tag{27}$$

where f_3 and f_2 are given by (6).

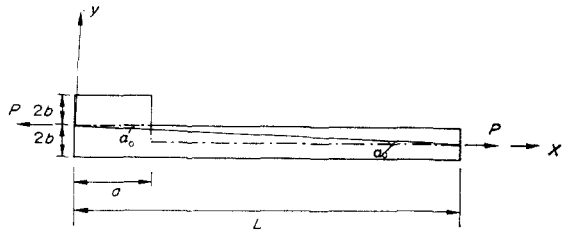

Fig. 4. Central section of the joint.

4. *Determination of* $\hat{\theta}$

The bonded portion of a lap joint experiences a rotation relative to the original configuration if the joint is subjected to tension-shear loading. Here, we employ the Goland–Reissner analysis ([1] or [4], p. 210) to determine this angle of rotation.

Choose the origin at the center of the bonded region and the x-axis in the direction of applied force, as shown in Fig. 4. Then, the initial configuration of the center line is

$$y(x) = \begin{cases} \dfrac{b}{L}x & x \in (0, a), \\ \dfrac{b}{L}x - b & x \in (a, L). \end{cases} \tag{28}$$

where b stands for the half thickness of the plate and L is the distance from the center of the joint to the point of load application.

Within the framework of elementary plate theory, the moment $M(x)$ and the governing differential equations for the displacement $v(x)$ of the center line in the y-direction are given by

$$M(x) = P[y(x) + v(x)] \qquad x \in (0, L), \tag{29}$$

$$\begin{aligned} &\frac{d^2v}{dx^2} - \frac{\kappa^2}{8b^2}[y(x) + v(x)] = 0 \qquad x \in (0, a), \\ &\frac{d^2v}{dx^2} - \frac{\kappa^2}{b^2}[y(x) + v(x)] = 0 \qquad x \in (a, L), \end{aligned} \tag{30}$$

where P is the magnitude of the applied force per unit width of the plate and

$$\kappa = \sqrt{\frac{3(1 - \nu^2)P}{2bE}}. \tag{31}$$

The boundary conditions to be adjoined to (30) are

$$\begin{aligned} &v(0+) = 0, \qquad v(L-) = 0, \\ &v(a-) = v(a+), \\ &\frac{dv}{dx}(a-) = \frac{dv}{dx}(a+). \end{aligned} \tag{32}$$

Now, the mean value of the angular change over the interval $(0, a)$ seems to be the most natural measure of the angle of rotation $\hat{\theta}$ of the joint employed in the preceding sections. We define $\hat{\theta}(\kappa, L)$ by

$$\hat{\theta}(\kappa, L) = \frac{b}{L} + \frac{1}{a}\int_0^a \frac{\mathrm{d}v}{\mathrm{d}x}\,\mathrm{d}x = \frac{b}{L} + \frac{v(a)}{a}. \tag{33}$$

Solving for v from (30) and (32) and then substituting into (33), we have

$$\hat{\theta}(\kappa, L) = \frac{b}{a}\cdot\frac{2\sqrt{2}}{2\sqrt{2} + \coth\left(\dfrac{\kappa a}{2\sqrt{2}\,b}\right)\tanh\left(\kappa\dfrac{L-a}{b}\right)}. \tag{34}$$

Finally, note from (34) that

$$\hat{\theta}(\kappa, L) = \tilde{\theta}(\kappa) + O\left(\exp\left(-2\kappa\cdot\frac{L-a}{b}\right)\right) \quad \text{as} \quad L \to \infty, \tag{35}$$

where

$$\tilde{\theta}(\kappa) = \frac{b}{a}\cdot\frac{2\sqrt{2}}{2\sqrt{2} + \coth\left(\dfrac{\kappa a}{2\sqrt{2}\,b}\right)}. \tag{36}$$

From now on we confine our discussion to the limiting case as $L \to \infty$.

5. *Numerical results, discussion*

We turn now to the numerical evaluation of the bond stresses via the integral equations (25). The kernels of these integral equations, K_1, and K_2, involve infinite integrals G_1, and G_2 defined by (27). To facilitate the numerical evaluation of G_1, we observe that

$$\begin{aligned} &\int_0^m f_3(s)\sin(\xi s)\,\mathrm{d}s = g_1(\xi, m) + O(m^5) \quad \text{as} \quad m \to 0, \\ &\int_M^\infty f_3(s)\sin(\xi s)\,\mathrm{d}s = O(\xi^2 \mathrm{e}^{-4M}) \quad \text{as} \quad M \to \infty, \end{aligned} \tag{37}$$

where

$$g_1(\xi, m) = \xi m - \frac{\xi m^2}{2} + \frac{\xi(4 - 15\xi^2)}{45}m^3 + \frac{\xi^3}{24}m^4. \tag{38}$$

Therefore, the values of G_1 may be evaluated to any desired degree of accuracy from

$$G_1(\xi) = g_1(\xi, m) + \int_m^M f_3(s)\sin(\xi s)\,\mathrm{d}s \tag{39}$$

by choosing suitable numbers for m and M and evaluating the integral by Filson's formula ([5], p. 890). The analogous approximate formula for G_2 is found to be

$$G_2(\xi) = g_2(\xi, m) + \int_m^M f_2(s)\sin(\xi s)\,\mathrm{d}s, \tag{40}$$

where

$$g_2(\xi, m) = -\frac{3\xi}{4m} + \left(\frac{3}{5} - \frac{\xi^3}{8}\right)m - \frac{\xi m^2}{2} + \left(\frac{64}{525}\xi - \frac{\xi^3}{30} + \frac{\xi^5}{480}\right)m^3 + \frac{\xi^3}{24}m^4. \tag{41}$$

As for the evaluation of the integrals appearing in the definitions of K_1 and K_2, we remove the contributions from the Cauchy-type singularities by use of the elementary integral

$$\int_0^\alpha \frac{\sqrt{s(\alpha - s)}}{s - \xi}\,\mathrm{d}s = \frac{\pi}{2}(\alpha - 2\xi) \qquad \xi \in [0, \alpha], \tag{42}$$

and evaluate the remaining regular integrals numerically.

To solve the integral equations (25), we introduce a uniform partition of the interval $[0, \alpha]$ and approximate the unknown functions by continuous functions that are linear in each subinterval. Subsequently, we evaluate the contributions over the first and the last interval, taking the square root singularities of the kernel into account, and employ the trapezoidal rule for the remainder. In this manner each of the integral equations (25) is reduced to an approximating system of linear algebraic equations for the values of $\hat{N}$ or $\hat{Q}$ at the mesh points of the underlying partition.

We proceed now to the discussion of illustrative numerical examples. The stress distribution in the present model of a lap joint under a tension-shear loading may be determined if the mean angle of rotation $\tilde{\theta}$ of the joint is given in addition to the parameter a/b which characterizes the geometry of the joint. This mean angle of rotation, in turn, depends exclusively upon the ratio a/b and the parameter κ defined by (31) within the current approximation. Figure 5 shows the dependence of $\tilde{\theta}$ on κ for $a/b = 4$, 6, 8 and 10, on the basis of (36). The dashed lines represent the maximum values of $\tilde{\theta}$ for given a/b values.

We note at this point that the solutions of the pair of integral equations (25) are related to the bond stresses through

$$\begin{aligned} \hat{N}(x_1/b) &= \frac{1}{P} \cdot \sqrt{a^2 - x_1^2} \cdot \tau_{22}(x_1, -b), \\ \hat{Q}(x_1/b) &= \frac{1}{P} \cdot \sqrt{a^2 - x_1^2} \cdot \tau_{12}(x_1, -b) \qquad x_1 \in (-a, a) \end{aligned} \tag{43}$$

as is apparent from (16), (23) and (24). The variations of $\hat{N}$ and $\hat{Q}$ are shown for $a/b = 8$

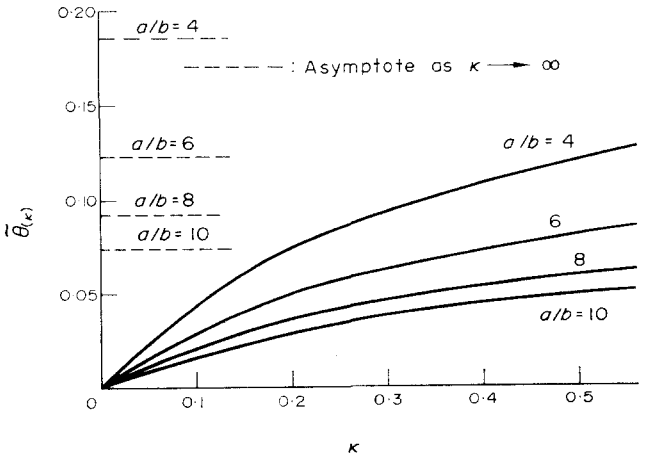

Fig. 5. Dependence of the rotation angle of the joint on κ.

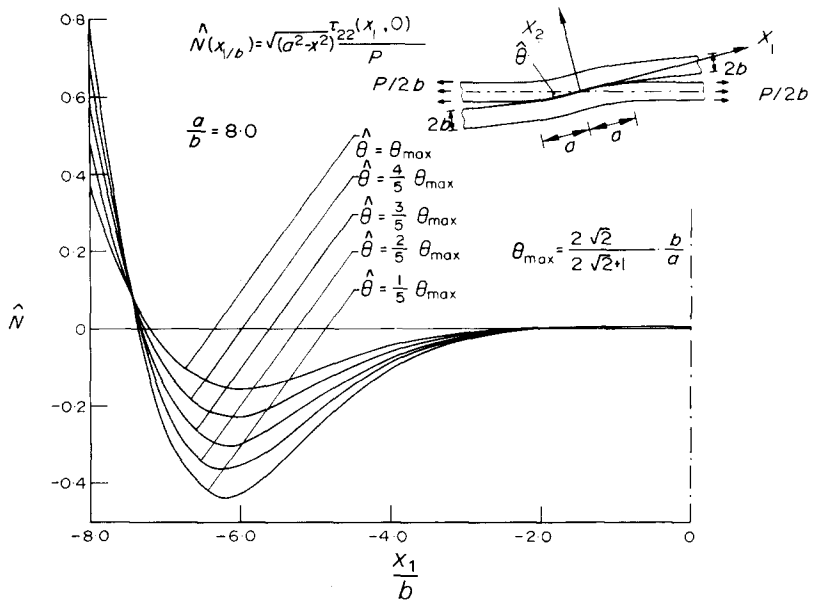

Fig. 6. Distribution of normalized normal bond stress.

on Figs. 6 and 7, respectively. For the mean angle of rotation, we employed here the values 1/5, 2/5, 3/5, 4/5 and 5/5 of the maximum possible angle of rotation under a tension-shear loading. Because $\hat{N}$ and $\hat{Q}$ are both even functions of x_1, only the variations of these quantities over half of the interval are shown.

In view of (43), we define next the stress intensity factors λ_1 and λ_2 by

$$\lambda_1 = \lim_{x\to a} \hat{N}(x_1/b) = \hat{N}(\alpha),$$
$$\lambda_2 = \lim_{x\to a} \hat{Q}(x_1/b) = \hat{Q}(\alpha). \tag{44}$$

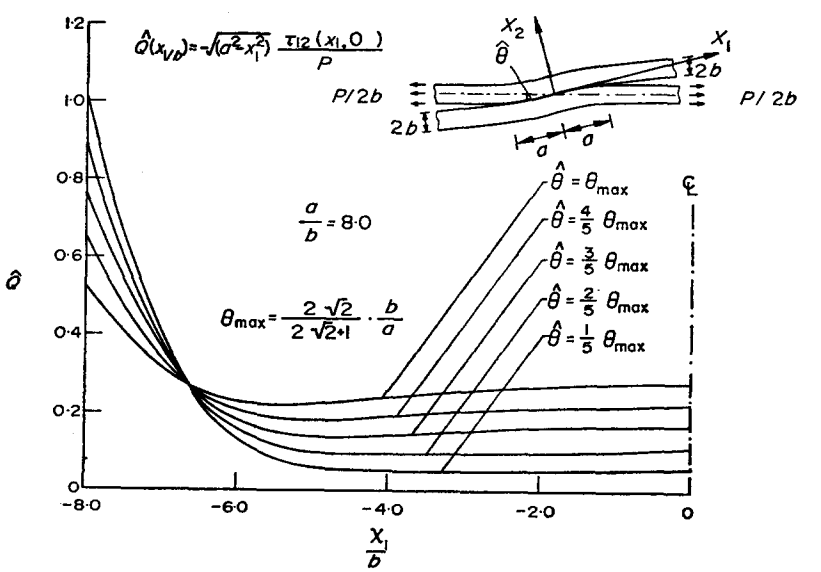

Fig. 7. Distribution of normalized shear bond stress.

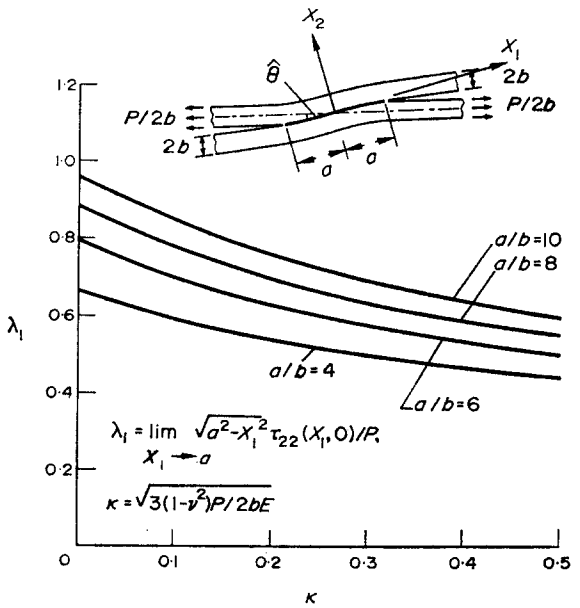

Fig. 8. Dependence of λ_1 on κ.

We should emphasize the dependence of λ_1 and λ_2 on the parameters κ and α. When κ and α are given, the angle of rotation of the joint can be determined from (36) and $\hat{N}$ and $\hat{Q}$ are then obtained by solving the integral equations (25). Figures 8 and 9, depicting the dependence of λ_1 and λ_2 upon κ for $\alpha = a/b = 4$, 6, 8 and 10, were prepared in this manner.

It is normal in lap joint construction to initially have a finite overlap that is completely bonded. This means that the joint as constructed contains no cracks and has a different geometry from the model presented here. This is especially important since crack initiation and growth at the ends of the bond line depend strongly upon the geometry of the adherends in these regions. A consideration of the geometrical effects at these points was attempted by Westmann[6].

On the other hand, a lap joint may experience slow crack growth due to cyclic thermal or mechanical loadings. Such cracks can initiate at the ends of the bond line and grow stably for some time. The resulting joint geometry is then quite similar to that of the problem considered here and the question as to the strength of the cracked joint may be answered using the present model.

The stress analysis completed in this paper is based upon the assumption that a state of plane strain exists. This two-dimensional approximation precludes the application of the results in regions near the sides of the joints.

The results presented here permit us to conduct a strength analysis of a joint where the cracks have extended from the initial ends of the bond line. The singular stress fields at the tips of the crack are characterized by the usual two stress intensity factors $\bar{K}_{\mathrm{I}}$, $\bar{K}_{\mathrm{II}}$ used in fracture mechanics. These quantities are related to λ_1, λ_2 in Figs. 8, 9 by

$$\bar{K}_{\mathrm{I,II}} = P \cdot \sqrt{\frac{\pi}{a}} \cdot \lambda_{1,2}. \tag{45}$$

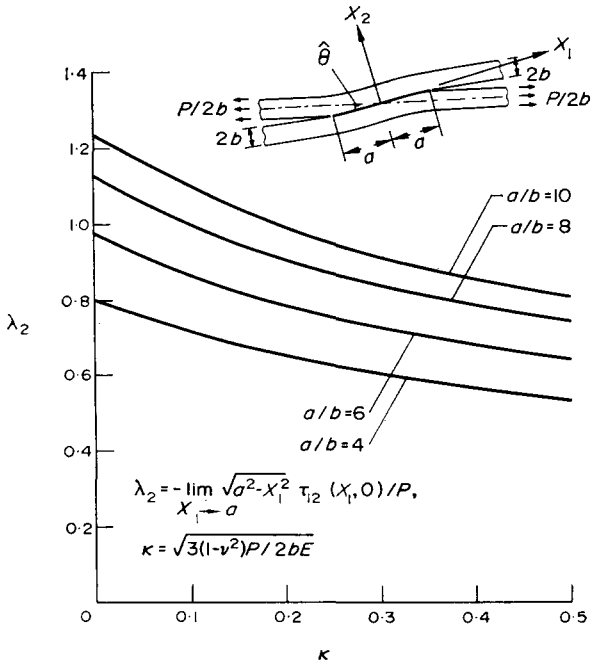

Fig. 9. Dependence of λ_2 on κ.

A knowledge of how unstable bond-line crack growth depends upon the combination of $\bar{K}_{\mathrm{I}}$, $\bar{K}_{\mathrm{II}}$ permits the completion of the strength analysis.

One way to accomplish this is to use the results of brittle fracture theory and the concept of a strain energy release rate $\mathscr{G}$. As developed by Irwin[7], this theory states that a crack will propagate when the change of strain energy of the system (for an infinitesimal increase in crack length) is equal to a critical material value $\mathscr{G}_c$ times the change in crack length.

If the crack propagates along the bond line, the direction of crack growth is known. This permits the expression of the strain energy release rate in terms of $\bar{K}_{\mathrm{I}}$, $\bar{K}_{\mathrm{II}}$,[8], as follows

$$\mathscr{G} = \frac{1-\nu^2}{E}(\bar{K}_{\mathrm{I}}^2 + \bar{K}_{\mathrm{II}}^2) = \frac{P^2\pi}{b} \cdot \frac{1-\nu^2}{E} \cdot \left[\frac{b}{a}(\lambda_1^2 + \lambda_2^2)\right] \qquad \text{(plane strain).} \tag{46}$$

The failure prediction is completed upon setting $\mathscr{G}$ equal to the material value $\mathscr{G}_c$. In this way the failure load P_c required to cause unstable crack growth is determined to be

$$P_c = \sqrt{\frac{E\mathscr{G}_c b}{1-\nu^2}} \left[\frac{a/b}{\pi(\lambda_1^2 + \lambda_2^2)}\right]^{1/2} \qquad \text{(plane strain).} \tag{47}$$

Figure 10 presents the dependence of the normalized force $\bar{P}$ defined by

$$\bar{P} = P_c \Big/ \sqrt{\frac{E\mathscr{G}_c b}{1-\nu^2}} \tag{48}$$

on the parameter κ for several values of a/b.

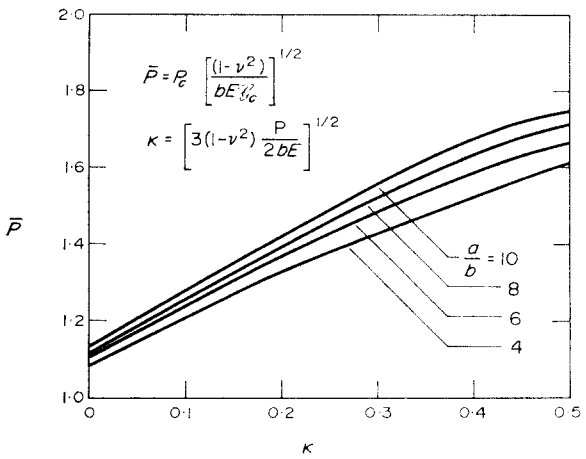

Fig. 10. Dimensionless strength of joint as a function of κ.

We now turn to the discussion of the use of Fig. 10. Observe first that the stress field does not depend upon the load P in a linear manner. Accordingly the strength analysis is not linear. For a given geometry and material (a/b, E, $\mathcal{G}_c$ fixed) the strength depends in a complicated way upon these parameters owing to the joint rotation and the parameter κ.

To see this, we assume that E, a/b and $\mathcal{G}_c$ are known and attempt to find P_c. To do so, we must know κ which in turn depends upon P_c. Thus one must first estimate κ and then obtain a first estimate for P_c (say $(P_c)_1$) from Fig. 10. The value of κ can now be recomputed and a new value $(P_c)_2$ determined from the figure. This process is repeated until $(P_c)_n = (P_c)_{n+1} = P_c$, which should not take more than a few iterations.

The dependence of the joint strength upon the geometry should be discussed in a little more detail. Observe from Fig. 10 that for a fixed adherend thickness $2b$ the dependence of $\bar{P}$ upon the bond length $2a$ is weak. The reason for this is that the bulk of the force transfer across the bond line occurs near the crack tips (see Figs. 6, 7) and hence increasing the bond line length does not significantly alter the stress field near these points.

On the other hand the adherend thickness $2b$ plays a more important role. For example, in the case $\kappa = 0$, the normalized strength $\bar{P}$ is approximately 1.1 for $a/b \in [4, 10]$. From equation (48) it is seen that the strength P_c is approximately proportional to $\sqrt{b}$. This suggests that a more efficient way to improve the strength of the joint is to increase the thickness of the adherends in the vicinity of the ends of the bond line.

In retrospect, this is to be expected upon recognition of the fact that, for $a/b \geq 4$, the force transfer across the bond line occurs primarily at the current ends of the bond. Only changes in the geometry near those points, i.e. changes in the adherend thickness $2b$, can affect this force transfer. Since $b = 0$ implies zero strength, increasing b must lead to an improvement of the strength characteristics of the adhesive joint. Of course, these comments only apply to the case where cracks have issued from the initial ends of the bond line and for those combinations of adhesives and adherends for which brittle fracture mechanics is applicable. In the event the adhesive material exhibits yielding the above model is not applicable and an alternate approach is necessary[9].

It is clear that the model of an adhesive joint presented here can be improved. For example, the effects of the adherend geometry at the initial ends of the bond line are of key

importance and should be included in any strength analysis of an uncracked connection. Nevertheless it is felt the results presented here are useful. The effect of the rotation of the joint with the resulting interaction between λ_1 and λ_2 has been demonstrated. At the same time it was possible to complete a simple strength analysis (within the scope of brittle fracture mechanics) and show the role of the geometric parameters upon the load carrying capacity of the adhesive lap connection.

Acknowledgement—This work was supported by the National Science Foundation under Grant GK-30773, at the University of California, Los Angeles. Also, the authors would like to thank R. A. Westmann for his helpful discussions.

REFERENCES

1. M. Goland and E. Reissner, The stresses in cemented joints, *J. Appl. Mech.* **11**, 17 (1944).
2. H. Y. Fan and R. Muki, Load transfer from a web to two parallel sheets, *Appl. Sci. Res.* **25**, 1 (1971).
3. N. I. Muskhelishvili, *Singular Integral Equations*. Noordhoff (1953).
4. D. D. Eley (Editor), *Adhesion*. Oxford University Press (1961).
5. A. Abramowitz and I. A. Stegun, *Handbook of Mathematical Functions*. Dover (1965).
6. R. A. Westmann, *Geometrical Effects in Adhesive Joints*, (in Preparation), Institut für Festkörpermechanik, Freiburg, Germany.
7. G. R. Irwin, Analysis of stresses and strains near the end of a crack traversing a plate, *J. appl. Mech.* **24**, 361 (1956).
8. J. R. Rice, *Mathematical Analysis in the Mechanics of Fracture*, Vol. 2, Chapter 3. Academic Press (1968).
9. R. A. Westmann, *An Elementary Model for Yielding and Slip in Adhesive Joints*, Report 1/73, Institut für Festkörpermechanik, Freiberg, Germany (1973).